

Moisture Transport and Diffusive Instability during Bread Baking

H. HUANG*, P. LIN[†] and W. ZHOU[‡]

June 9, 2006

Abstract

In this paper we study two related multiphase models for simultaneous heat and mass transfer process during bread baking. Our main objective is to provide an explanation and a remedy to the observed erroneous and/or divergent results associated with the instantaneous phase change model used in the literature. We propose a reaction-diffusion model based on the Hertz-Knudsen equation, where the phase change is not instantaneous but determined by an evaporation/condensation rate. A splitting scheme is designed so that a relation between these two models can be established and the non-intuitive numerical instability associated to the instantaneous phase change model can be identified and eliminated through the reaction-diffusion model. The evaporation/condensation rate is estimated from balancing these two models and reasonable and consistent results are produced by using the estimated rate. For the evaporation/condensation rate beyond the estimated value oscillation, solutions with multiple regions of dry and two-phase zones is observed. We show that these are caused by an instability intrinsic to the model (which we call diffusive instability) and the effect of the diffusive instability to the bread-baking simulation is also explained through a linear stability analysis and supported by numerical tests.

Keywords: Multi-phase Modeling, Heat and Mass Transfer, Phase Change, Reaction-Diffusion Equation, Diffusive Instability, Finite Difference Method, Linear Stability Analysis.

1 Introduction

Bread baking process is difficult to model, partly due to the fact that simultaneous heat and mass transfer are involved during the process. During baking, heat transfer in dough is

*Department of Mathematics and Statistics, York University, Toronto, Ontario, Canada M3J 1P3. hhuang@yorku.ca

[†]Department of Mathematics, National University of Singapore, Singapore 117543. matlinp@nus.edu.sg

[‡]Food Science and Technology Programme, Department of Chemistry, National University of Singapore, Singapore 117543. chmzwb@nus.edu.sg

a combination of conduction/radiation from band or tins to the dough surface, convection from air to the dough surface in the absence of baking tins, conduction in the continuous liquid/solid phase of the dough, and evaporation-condensation in the gas phase of the dough.

De Vries et al. [8] described a 4-step mechanism for the heat transport inside dough: (1) water evaporates at the warmer side of a gas cell that absorbs latent heat of vaporization; (2) water vapour then migrates through the gas phase; (3) when meeting the cooler side of the gas cell, water vapour condenses and becomes liquid; (4) finally heat and water are transported by conduction and diffusion through the gluten gel to the warmer side of the next cell. The water diffusion mechanism becomes important to heat transfer, because dough tends to be a poor conductor that limits the heat transfer rate via conduction.

The above described mechanism of diffusion together with evaporation and condensation in dough was subsequently adopted by Tong and Lund [19] and Thorvaldsson and Janestad [18]. With this mechanism, liquid water moved towards the loaf centre as well as the surface by evaporation and condensation, reducing the partial water vapour pressure due to the temperature gradient. As a result, crumb temperature increasing was accelerated.

In the model by Zanoni et al. [20], an evaporation front inside the dough was assumed to be always at 100°C. This evaporation front progressively advanced towards the centre as bread's temperature increased. Crust was formed in the bread portion above the evaporation front. With similar parameters, Zanoni et al. [21] developed a 2-dimensional axi-symmetric heat diffusion model. The phenomena were described separately for the upper and lower parts (crust and crumb). The upper part (crust) temperature was determined by equations including heat supply by convection, conductive heat transfer towards the inside, and convective mass transfer towards the outside. The lower part (crumb) temperature was determined by the Fourier's law. In addition to the Cartesian co-ordinate models, a 1-dimensional cylindrical co-ordinate model was also established by De Vries et al. [8].

Among the various models, the internal evaporation-condensation mechanism well explains the fact that heat transfer in bread during baking is much faster than that described by the conduction alone in dough/bread. It also supports the observation that there is an increase in the liquid water content at the centre of bread during the early stage of baking (Thorvaldsson and Skjoldebrand [17]), rather than a monotonous decrease resulted from having liquid water diffusion and surface evaporation only. Therefore, a promisingly good model for bread baking might be a multiphase model which consists of three partial differential equations for the simultaneous heat transfer, liquid water diffusion and water vapour diffusion respectively, together with two algebraic equations describing water evaporation and condensation in the gas cells. Indeed, Thorvaldsson and Janestad [18] used this multiphase model to describe a one-dimensional case where baking tin was absent.

In [18], a slab of bread crumb being baked in a conventional oven was considered. The model assumed that the vapor and liquid water diffused separately and the phase change (evaporation and condensation) occurred instantaneously, i.e., the vapor content V was directly proportional to the saturated vapor content V_s at the same temperature at any given time, provided that there was enough liquid water available. The authors showed reasonably good agreement between the numerical results predicted by the model and the

experimental measurements. However, further investigations using the same model revealed that the numerical procedure for solving the model became a serious issue as the time step size is refined [15, 22].

Zhou [22] demonstrated that numerically solving the model presented a big challenge. Although various schemes of finite difference methods (FDM) and finite element methods (FEM) were applied, the corresponding solutions were all shown to be highly sensitive to the time step and satisfactory results were only yielded over a limited range of time step. Erroneous and/or divergent results were produced when the time step size was either too small or too large. While it is reasonable to expect that large time step may lead to instability, failure of the numerical methods due to small time step sizes is non-intuitive.

The main objective of this paper is to provide an explanation as well as a remedy to this highly non-intuitive outcome of the instantaneous phase change model. We start by re-examining the model and the numerical procedures used in [18, 15, 22]. In order to identify the source of instability occurred in the instantaneous phase change model, we construct a reaction-diffusion model by assuming that the phase change follows a modified Hertz-Knudsen equation, which can be derived using statistical mechanics principles [12]. We show that the two models are equivalent from a numerical point of view, when a special time stepping scheme is used for the reaction-diffusion model, by selecting an evaporation rate reciprocal to the time step size. Therefore, reducing the time step size in the instantaneous phase change model is equivalent to refining the time step as well as increasing the evaporation rate in the reaction-diffusion model.

The reaction-diffusion model allows us to study the effects of the evaporation rate in more details by separating two types of instabilities, i.e., instability associated with the particular numerical scheme and an intrinsic diffusive instability associated with the model. Combining numerical tests and linear stability analysis, we show that the diffusive instability is an intrinsic feature of the model, which does not disappear as the time step is reduced. As a result, the two-phase region where vapor and liquid water co-exists, may become unstable. For the parameter values used in [18, 15, 22], the constant state solution in the two-phase region is linearly unstable even though the solution is stable when the phase change and diffusion are considered separately. Furthermore, the rate of growth depends on the evaporation rate. A larger evaporation rate leads to faster growth of the disturbances. Oscillation in solutions can occur in the two-phase region before the dry region completely takes over.

We show that the reaction-diffusion model does not lead to numerical instability when sufficiently small time step size is used. In the instantaneous phase change model, reducing the time step size is equivalent to increasing the evaporation rate while keeping the ratio of the time step size and the evaporation rate fixed. Therefore, systematic refinement of the time step size induces faster growth of error, which eventually causes numerical instability observed in the computations in [15, 22].

In order to put the problem we study in this paper in a broader context, we shall give a brief overview of some relevant applications whose mathematical description has certain similarity to the bread baking models discussed here. A general feature of these problems is the coupling of thermal diffusion and phase change. We refer to [3, 4, 5, 6, 9] for treatments of

phase change and heat transfer phenomena in general. A closely related application is given in [14, 13], where a moisture transport model for the wetting and cooking of a cereal grain is considered. The temperature is decoupled from the moisture model and it is used as a parameter in their model. In [11, 10], the condensed phase combustion or gasless combustion is considered. The model has applications in synthesizing certain ceramics and metallic alloys and involves a reaction-diffusion system for the temperature and the concentration of the fuel, where the diffusion coefficient of the fuel concentration is set to be zero. In [2], a model for the aggregate alkali reaction in fluid leaching processes, which is similar to the gasless combustion, is studied numerically. All these models are similar to the one studied in [18, 15, 22], with some differences in the way the phase change is handled and in the parameters and coefficients. Numerical techniques used in those studies are also similar, where either finite difference and finite element methods or pseudo-spectral method are used for the spatial discretization.

The rest of the paper is organized as follows. In section 2 we revisit the instantaneous phase change model used in the literature for bread baking application and show its inconsistent result when the time step is reduced. In section 3, we propose a reaction-diffusion model based on the Hertz-Knudsen equation. The relationship between the two models will be explored in section 3.2 when the numerical method is discussed. Numerical results of the reaction-diffusion model are given in section 3.3. In section 4 we carry out the linear stability analysis of our new model. We finish the paper by a conclusion and a short discussion on future directions in section 5.

2 The Instantaneous Phase Change Model

The multiphase model used and studied in [18, 15, 22] assumes that the bread can be treated as a homogenous porous medium with density ρ , specific heat capacity c_p , thermal conductivity k . While both c_p and k are assumed to be constants, density ρ is given as a function of the liquid water content. The main variables are T , V and W , where T is the temperature in K , W and V are the liquid water and water vapor content (defined as the percentage of vapor and liquid water mass, compared to that of the mixture including the bread) inside the bread with respect to the total weight (unit-less). Thus the total vapor and liquid water masses per unit of volume can be computed as ρV and ρW , respectively. The vapor and liquid water can be generated via evaporation and condensation, respectively, determined by the saturated vapor concentration $V_s(T)$, which is temperature dependent. The evaporation and condensation is assumed to be instantaneous. The vapor and liquid water can also be transported via diffusion, with coefficients D_V and D_W , respectively. We note that only vapor and liquid water in the pore are being considered in this model and as well a modified model to be discussed.

It is assumed that the bread has certain moisture content W_0 (liquid water) at the room temperature T_0 initially. At time zero, the bread is placed in an oven pre-heated at temperature T_a by a radiator at temperature T_r .

Based on these assumptions and the conservation laws, the governing equations can be

written down as

$$\rho c_p T_t = (kT_x)_x + \lambda \Gamma, \quad (1)$$

$$V_t = (D_V V_x)_x, \quad (2)$$

$$W_t = (D_W W_x)_x \quad (3)$$

where λ is the latent heat of phase change and Γ is the mass rate of phase change. We note that rate of change in vapor and liquid water included in the above equations is due to diffusion only with the assumption that the local equilibrium is maintained by instantaneous phase change in the two-phase region.

To be more precise, consider a time instant when vapor and water content, denoted by V and W , with temperature T , which are not at an equilibrium. This leads to either evaporation or condensation and the equilibrium state will be restored and the vapor content is given by

$$V^* = cV_s(T) \quad (4)$$

if there exists sufficient amount of liquid water in the case of evaporation. Here c is a phase change constant whose value is determined by comparing the computational result and the experiment result given in [18]. The amount of phase change (mass) can be computed as

$$\Gamma = \rho(V^* - V) \equiv \rho[cV_s(T) - V]$$

as long as $\Gamma < \rho W$. The amount of liquid water after the phase change is given by

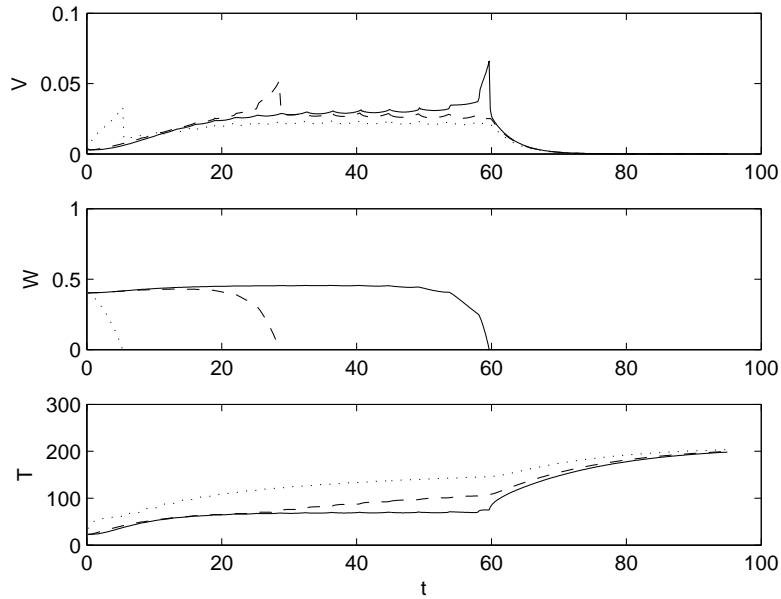
$$W^* = W - \frac{\Gamma}{\rho}.$$

On the other hand, if $\Gamma \geq \rho W$, the phase change (mass) is given by

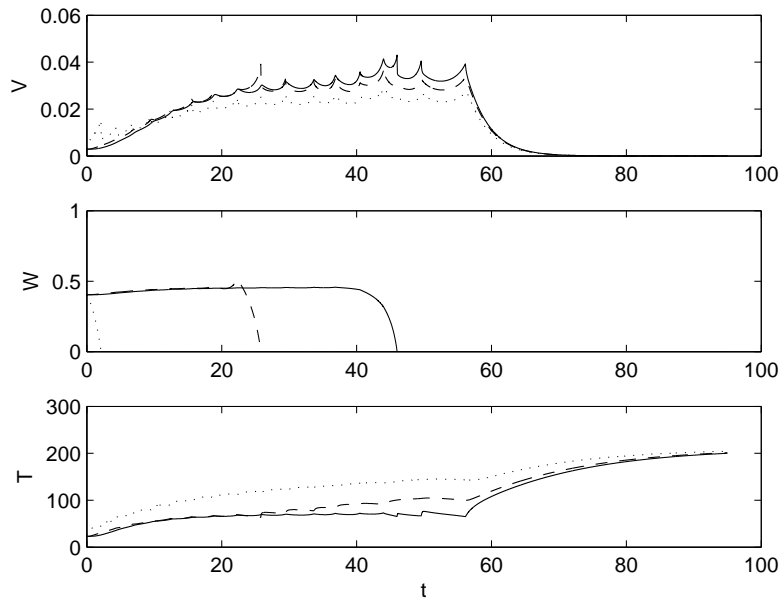
$$\Gamma = W$$

with $W^* = 0$ and $V^* = V + W$.

An implicit assumption made in the model described above is that the phase change occurs at a much shorter time scale than the diffusion, which is valid in general. When a numerical method is used to solve the model equations, instantaneous phase change also implies that the time scale for phase change is shorter than any time step sizes taken in the computation, which may not be valid as the time step size becomes small. In Figure 1, we have reproduced some of the computations based on the geometric and boundary conditions in [22]. Initially the vapor and liquid water content as well as the temperature are assumed to be uniformly distributed within the bread slab. As a higher temperature is imposed at the boundary $x = 0$, the temperature inside the bread will rise, causing water to evaporate near the boundary. The vapor diffuses towards the center of the bread ($x = L$) and condenses as the temperature is lower there, which leads to an increased amount of liquid water. In Figure 1, we plot V , W and T at three locations $x = 0$, $L/2$, and L . The computational



(a)



(b)

Figure 1: *Computational results of V , W , and T obtained by using the instantaneous phase change model. Time step sizes are (a) $\Delta t = 10$ seconds; (b) $\Delta t = 1$ second. In this figure as well as in Figures 3 and 4, the dotted lines represent the quantities at the surface of the slab ($x = 0$), the dashed lines are for those located in the middle of the domain ($x = L/2$) and the solid lines represent the values at the center of the slab ($x = L$). The time is measured in minutes.*

results show that a perfectly reasonable solution can be obtained when the time step is $\Delta t = 10$ sec (Figure 1a). A systematic refinement of the time step eventually causes the solution to diverge (e.g. $\Delta t = 1$ sec depicted in Figure 1b). The solution blows up when the time step size is further reduced to $\Delta t = 0.5$ sec.

The results in Figure 1 are obtained using an implicit Euler time stepping scheme while the second order center finite difference scheme is used to approximate the spatial derivatives. These results are consistent with those observed earlier where both first order and second order time stepping methods were used [22]. Relatively coarse grids (16 points) are used in the x direction since a finer grid also leads to numerical instability.

In Figure 2, we provide more numerical evidence by plotting the maximum norm of the computed water content W as a function of time, as the time step size and spatial grid size are systematically refined. As shown in the figure, the numerical solution grows as the time and spatial step sizes are refined. Eventually the solution grows out of bound when the step sizes are further refined, indicating instability in the numerical solution.

The instability due to spatial step size reduction is likely to be numerical. However, the loss of stability by reducing the time step size is counter-intuitive. From numerical analysis point of view, reducing time step size normally stabilizes time step schemes. Therefore, the loss of stability is likely due to other effects. As revealed by our analysis in the subsequent sections, the numerical instability observed in the computations can be attributed to an intrinsic feature of the model, due to the interplay of heat and mass diffusion and the phase change. We note that the numerical results presented here are in dimensional form, for easy comparison with those given in the literature. It is worth pointing out that the scale of the time step sizes is much smaller than the diffusive time scale, which is on the order of 10^3 seconds. The time scale for the phase change, on the other hand, should be smaller than the time step sizes in order for the phase change to be “instantaneous”.

3 A Reaction-Diffusion Model

Since the instantaneous phase change model does not seem to lead a satisfactory solution, we now consider an alternative model which does not assume instantaneous phase change. In particular, we shall study the following reaction-diffusion model which is similar to that in the previous section except that the phase is not instantaneous. The governing equations of the model are again the conservation of mass and energy.

$$\rho c_p \frac{\partial T}{\partial t} = \frac{\partial}{\partial x} \left(k \frac{\partial T}{\partial x} \right) + \lambda \Gamma, \quad (5)$$

$$\frac{\partial V}{\partial t} = \frac{\partial}{\partial x} \left(D_v \frac{\partial V}{\partial x} \right) - \frac{\Gamma}{\rho}, \quad (6)$$

$$\frac{\partial W}{\partial t} = \frac{\partial}{\partial x} \left(D_w \frac{\partial W}{\partial x} \right) + \frac{\Gamma}{\rho} \quad (7)$$

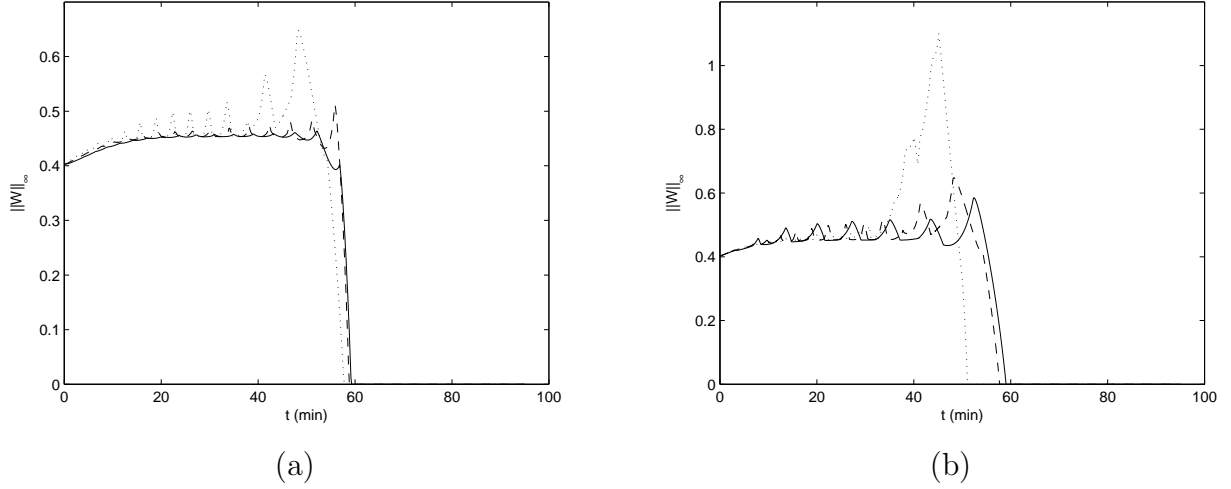


Figure 2: Maximum norm of the computed water content is plotted as a function of time (measured in minutes). (a). The solid, dashed and dotted lines are solutions obtained using time step sizes $\Delta t = 5, 2.5,$ and 1.25 seconds while the number of grid in x is fixed at $N = 16$; (b). The solid, dashed and dotted lines are solutions obtained using $N = 8, 16, 32$ grid points in x while the time step size is fixed as $\Delta t = 0.625$ seconds.

for $0 < x < L$. Here Γ is the rate of the phase change (mass per unit volume per unit time). It is through Γ that our model differs from the one in the previous section. We assume that it is given by the modified Hertz-Knudsen equation (See [12] where this equation is used for studying evaporation phenomenon).

$$\Gamma = E(1 - \phi) \sqrt{\frac{M}{2\pi R}} \frac{(P_v - cP_s)}{\sqrt{T}} \quad (8)$$

where E is the condensation/evaporation rate, ϕ is the porosity of the bread slab, M is the molecular weight of water and R is the universal gas constant, P_v and P_s are the vapor pressure and saturation pressure, and c is another phase change constant same as the model in the previous section. For simplicity we have included the pore surface area in E , which is inversely proportional to the pore size of the porous sample. Even for a unit pore surface, the value of evaporation rate E is subject to debate [12]. In this study, we will estimate the value of E by comparing the current model with the instantaneous phase change one in the next section.

Assuming the ideal gas law,

$$P_v = \frac{R\rho_v T}{\phi M}, \quad P_s = \frac{R\rho_s T}{\phi M} \quad (9)$$

we can re-write (8) as

$$\Gamma = \frac{E(1-\phi)\rho}{\phi} \sqrt{\frac{RT}{2\pi M}} (V - cV_s). \quad (10)$$

Following [18, 15, 22], the boundary conditions are mixed condition at $x = 0$:

$$-k \frac{\partial T}{\partial x} = h_r(T_r - T) + h_c(T_a - T) - \lambda \rho D_w \frac{\partial W}{\partial x}, \quad (11)$$

$$-\frac{\partial V}{\partial x} = h_v(V_a - V), \quad (12)$$

$$-\frac{\partial W}{\partial x} = h_w(W_a - W) \quad (13)$$

and symmetric condition at $x = L$:

$$\frac{\partial T}{\partial x} = \frac{\partial V}{\partial x} = \frac{\partial W}{\partial x} = 0. \quad (14)$$

Here h_r , h_c , h_v and h_w are the radiative, convective heat transfer coefficients, vapor and liquid water mass transfer coefficients. V_a and W_a are the vapor and liquid water content in the oven air. The values of parameters relevant to bread baking are given in the Appendix.

3.1 Nondimensionalization

We now proceed to nondimensionalize the equations by choosing the following scaling

$$\theta = \frac{T - T_0}{\bar{T}}, \quad \tau = \frac{t}{\bar{t}}, \quad \xi = \frac{x}{L}, \quad \rho' = \frac{\rho}{\bar{\rho}}.$$

Here $T_0 = 298.15 \text{ K}$ is the initial temperature and $\bar{T} = T_r - T_0$ is the difference between the radiator and initial temperature. $\bar{\rho} = 284 \text{ kg/m}^3$ is the density of the flour. We choose the diffusive time scale for the temperature equation

$$\bar{t} = \frac{\bar{\rho} c_p L^2}{k}.$$

Drop the prime for simplicity and we have the following equations

$$\theta_\tau = \frac{1}{\rho_0 + W} \theta_{\xi\xi} + S, \quad (15)$$

$$V_\tau = D_1 [(\theta + \theta_0)^2 V_\xi]_\xi - \alpha S, \quad (16)$$

$$W_\tau = D_2 W_{\xi\xi} + \alpha S \quad (17)$$

where $\rho_0 = \rho(0)/\bar{\rho}$,

$$D_1 = \frac{D_{V0} \bar{\rho} \bar{T}^2 c_p}{k}, \quad D_2 = \frac{D_W \bar{\rho} c_p}{k}, \quad \alpha = \frac{\bar{T} c_p}{\lambda}.$$

The source term for the phase change is now

$$S = \beta\sqrt{\theta + \theta_0}(V - cV_s) \quad (18)$$

where

$$\beta = \lambda E(1 - \phi)\frac{\bar{\rho}L^2}{\phi k}\sqrt{\frac{R}{2\pi M\bar{T}}},$$

the saturated vapor content is

$$V_s = \frac{V_{s,0}e^{\gamma\theta} - V_{s,1}}{(\rho_0 + W)(\theta + \theta_0)},$$

with the parameters

$$V_{s,0} = \frac{P_{s,0}M}{\bar{\rho}\bar{T}R}, \quad V_{s,1} = \frac{P_{s,1}M}{\bar{\rho}\bar{T}R}, \quad \gamma = \kappa\bar{T}.$$

Note that we have fitted the saturated vapor pressure data [16] by an exponential function

$$P_s = P_{s,0} \exp[\kappa(T - T_0)] - P_{s,1}. \quad (19)$$

The nondimensional density is given as

$$\rho = W + \rho_0.$$

The boundary conditions at $x = 0$ and $x = L$ are nondimensionalized similarly. At $\xi = 1$ ($x = L$), we have

$$\theta_\xi = V_\xi = W_\xi = 0. \quad (20)$$

At $\xi = 0$ ($x = 0$), we have

$$\theta_\xi = (h_3 + h_4)(\theta - 1), \quad (21)$$

$$V_\xi = h_1(V - V_a), \quad (22)$$

$$W_\xi = h_2(W - W_a) \quad (23)$$

where

$$\begin{aligned} h_1 &= h_V L, \\ h_2 &= h_W L, \\ h_3 &= \frac{\sigma\bar{T}^3 L}{k} \frac{[(1 + \theta_0)^2 + (\theta + \theta_0)^2](\theta + 1 + 2\theta_0)}{\epsilon_p^{-1} + \epsilon_r^{-1} - 2 + F_{sp}^{-1}}, \\ h_4 &= \frac{h_c L}{k}. \end{aligned}$$

Here we have assumed that the air temperature T_a equals to the radiator temperature T_r .

Remark 1. Based on the parameter values relevant to bread baking given in the Appendix, we note that the diffusivity for vapor D_1 is bigger than that for the temperature by a factor of 5 while the diffusivity for liquid water is three orders of magnitude smaller. Thus, water is essentially immobile compared to that of vapor and temperature. In addition, transfer coefficients at the boundary is much smaller for liquid water than vapor by three orders of magnitude, while it is comparable for temperature. Thus, liquid water loss at the boundary can be neglected as well.

Remark 2. We have ignored the phase change at the boundary since its effect is small.

3.2 Numerical Method

We now turn our attention to the numerical solutions of the two models. In the following, we first describe a splitting scheme for the reaction-diffusion model.

3.2.1 Splitting scheme

When the instantaneous phase change model is used, we treat the diffusion equations of T , V and W and the phase change processes separately. For easy comparison we adopt a splitting method for the reaction-diffusion model by separating the diffusion from the phase change (reaction) term and solving the equations in two steps¹. We first solve the vapor and liquid water equations by

$$V_\tau = -\alpha S, \quad (24)$$

$$W_\tau = \alpha S. \quad (25)$$

The second equation for liquid water can be replaced by an algebraic constraint

$$V + W = V^0 + W^0$$

where V^0 and W^0 are the values at the beginning of the splitting step. Diffusion of vapor and liquid water as well as the temperature equation are solved in the second step by

$$\theta_\tau = \frac{1}{\rho_0 + W} \theta_{\xi\xi} + S, \quad (26)$$

$$V_\tau = D_1 [(\theta + \theta_0)^2 V_\xi]_\xi, \quad (27)$$

$$W_\tau = D_2 W_{\xi\xi}. \quad (28)$$

¹From the numerical method point of view, there is also a benefit to use the splitting. Since we can obtain an explicit relation between W and V in the phase change stage, W can be computed using V without treating the source term S in the W equation (or with that relation the source term in the W equation can be written in terms of W and is dissipative). As a result, the algorithm is more stable. We note that time splitting schemes have been used in the literature for reaction-diffusion equations and we refer interested readers to [1, 7] and references therein

3.2.2 Time stepping scheme

The numerical procedure in semi-discrete form can be described as follows.

1. We solve for vapor content first using

$$V_\tau = -\alpha S,$$

or

$$\frac{V^* - V^{(n)}}{\Delta\tau} = -\alpha\beta\sqrt{\theta + \theta_0}(V^{**} - cV_s^{(n)}) \quad (29)$$

where * denotes the solution updated due to phase change alone and ** indicates an average to be defined below.

2. Evaporation can only occur if there exists sufficient amount of the liquid water. In other words, liquid water content must remain non-negative. Therefore, liquid water content is updated using the constraint

$$W^* = \max\{W^{(n)} + V^{(n)} - V^*, 0\}. \quad (30)$$

3. As a consequence, vapor content is corrected using the constraint

$$V^* = W^{(n)} + V^{(n)} - W^*. \quad (31)$$

4. Phase change is computed using

$$\alpha S = \frac{W^* - W^{(n)}}{\Delta\tau}. \quad (32)$$

5. $V^{(n+1)}$ and $W^{(n+1)}$ are updated using the diffusion equations

$$\frac{V^{(n+1)} - V^*}{\Delta\tau} = (D_v V_\xi^{(n+1)})_\xi, \quad (33)$$

$$\frac{W^{(n+1)} - W^*}{\Delta\tau} = (D_w W_\xi^{(n+1)})_\xi. \quad (34)$$

6. Update the temperature

$$\frac{\theta^{(n+1)} - \theta^{(n)}}{\Delta\tau} = (D_T \theta_\xi^{(n+1)})_\xi - \beta\sqrt{\theta + \theta_0}(V^{**} - cV_s^{(n)}). \quad (35)$$

3.2.3 Model comparison

Note that the diffusion part of the reaction-diffusion model (26)-(28) are the same as that for the instantaneous model (1)-(3), in dimensionless form. The only difference between the reaction-diffusion model and the instantaneous phase change model lies in the way the phase change is computed, or more precisely the way vapor concentration V^* is computed. In the instantaneous phase change model, instead of solving (29), we set

$$V^* = cV_s. \quad (36)$$

We now show that this is a special case of the reaction-diffusion model.

When V^{**} is computed using arithmetic average, i.e.,

$$V^{**} = \frac{V^* + V^{(n)}}{2}, \quad (37)$$

we obtain

$$V^* - V^{(n)} = -\nu(V^* + V^{(n)} - 2cV_s^{(n)})$$

where

$$\nu = \frac{\Delta\tau\alpha\beta\sqrt{\theta + \theta_0}}{2}.$$

When $\nu = 1$, or

$$\beta = \frac{2}{\Delta\tau\alpha\sqrt{\theta + \theta_0}}, \quad (38)$$

which yields

$$V^* = cV_s^{(n)}.$$

Therefore, we show that the instantaneous phase change model is numerically equivalent to the reaction-diffusion model with a variable β inversely proportional to the time step size $\Delta\tau$.

3.3 Numerical Results

To simulate the moisture transport during bread baking we need to determine the evaporation/condensation rate E or its nondimensionalized quantity β . Since the main objective of the paper is to reveal the cause of the numerical instability associated with the instantaneous phase change model, we will not attempt to estimate the true value of E for bread baking. Instead, we first choose a time step size for which the instantaneous phase change model generates the “right” solution (comparable to experimental measurement). We then use (38) to determine evaporation/condensation rate. From numerical experiments in section 2 we choose the time scale $\Delta t = 10$ sec. Other parameter values may be found in Tables 1 and 2. We can thus estimate the value of β as

$$\beta \approx \frac{2\bar{t}}{\Delta t\alpha\sqrt{\theta_0}} = 781,$$

and the corresponding evaporation rate is $E = 4.5 \times 10^{-3}$. We can now carry out numerical computation with E fixed while refining the grid size in x and reducing the time step size until solution converges. In Figure 3, the numerical results based on this evaporation rate is given for two time step sizes $\Delta t = 10$ and 0.2 second using a coarse grid (16 grid points in x) and a fine grid (128 grid points in x), respectively. The numerical procedure remains stable as the time step is refined for a fixed grid size in x , contrary to the instantaneous phase change model. We note that the non-smoothness of the solution in Figure 3a is due to the coarse spatial and temporary grids used in the computation. When we refined the spatial grid, the solution becomes smooth, as shown in Figure 3b. In comparison to Figure 1a we also notice that the reaction-diffusion model and the instantaneous phase-change model indeed produce the same result when β satisfies (38).

Recall that reducing the time step size in the instantaneous phase change model is equivalent to increase the value of E in the reaction-diffusion model. Therefore, we can understand the mechanism of the instability associated with the instantaneous phase change model by carrying out the computations using a larger value of E . In Figure 4, computational results using the reaction-diffusion model with $E = 0.0045$ and $E = 0.045$ are presented. Here we plot the snap shots of the water content at various times in order to show what can happen with the model if we increase E . The results are obtained using 128 grid points in the x variable and a time step size of 0.2 second. We have also done further refinement tests but the results remain virtually the same, indicating convergence of the numerical solutions. Since we have decoupled the evaporation rate from the time step size, we can use a much smaller time step size while keeping the evaporation rate unchanged, which is not possible for the instantaneous phase change model. From Figure 4, it can be seen that the solution for the larger evaporation rate starts to oscillate. However, this is not due to numerical instability. In the next section we will provide an explanation of the oscillation and the instability caused by large E in the reaction-diffusion model (or small Δt in the instantaneous phase change model when the numerical procedure is still stable).

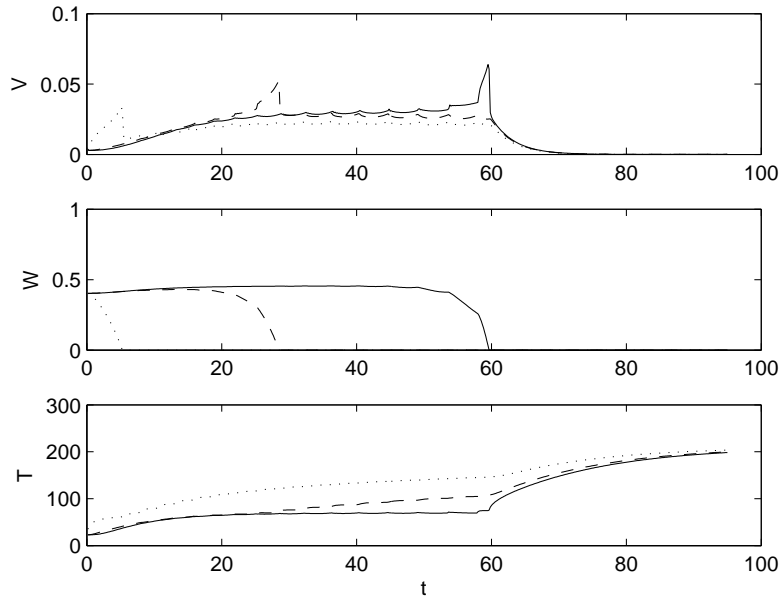
4 Linear Stability Analysis

Consider the stability near a steady state solution of the nondimensional model (15)-(17) in an infinite domain. It is easy to see that the constant state V_0 , W_0 and $\theta = 0$ satisfies the equations as long as

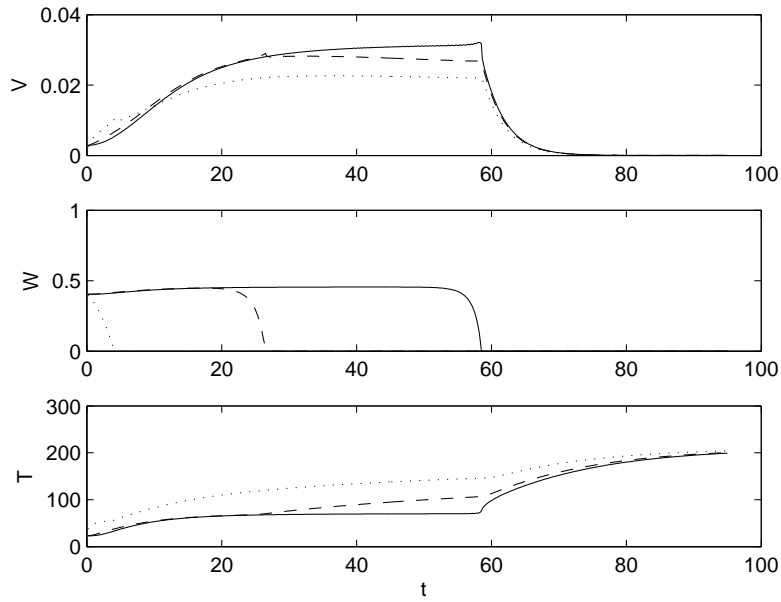
$$V_0 = \frac{c(V_{s,0} - V_{s,1})}{\theta_0(\rho_0 + W_0)}.$$

To verify the stability of the constant state solution, we carry out linear stability analysis by assuming that

$$\theta = \hat{\theta} \exp(s\tau + im\xi), \quad V = V_0 + \hat{v} \exp(s\tau + im\xi), \quad W = W_0 + \hat{w} \exp(s\tau + im\xi).$$



(a)



(b)

Figure 3: Computational results of V , W , and T obtained by using the reaction-diffusion model: (a). Time and spatial step sizes are $\Delta t = 10$ sec and $\Delta x = 2^{-4} \times 10^{-2}$ cm; (b). Time and spatial step sizes $\Delta t = 0.1$ sec and $\Delta x = 2^{-8} \times 10^{-2}$ cm.

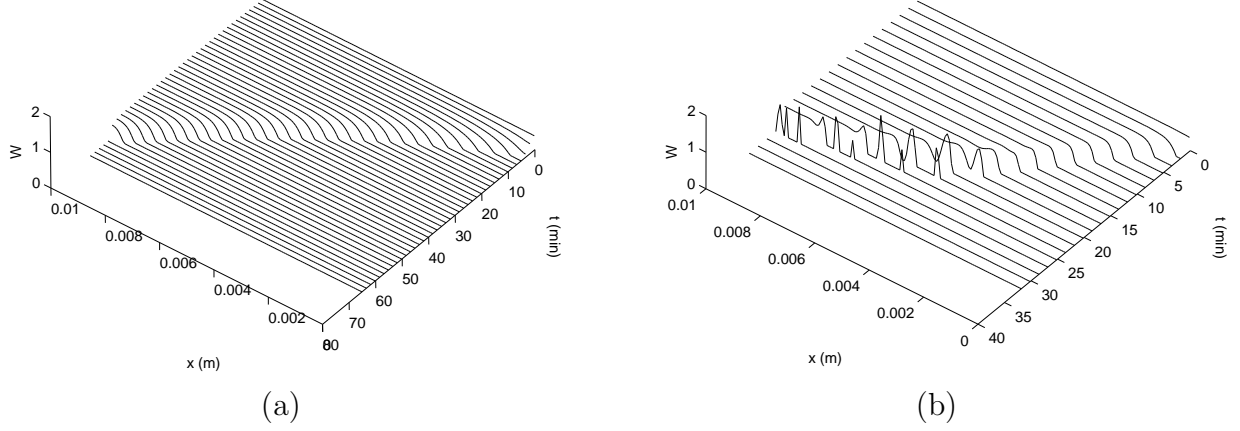


Figure 4: Snap shots of the water content computed using the reaction-diffusion model for two values of the evaporation constant: (a). $E = 0.0045$; (b). $E = 0.045$. For the smaller value of E , the water content remains monotonic in x and the interface between the dry and wet regions is clearly defined. For the larger value of E , disturbance from the interface grows and eventually leads to multiple dry-wet regions.

The equations for $\hat{\theta}$, \hat{v} and \hat{w} are

$$s\hat{\theta} = -\frac{m^2}{\rho_0 + W_0}\hat{\theta} + \bar{\beta} \left(-V_1\hat{\theta} + \hat{v} + \frac{V_0}{\rho_0 + W_0}\hat{w} \right), \quad (39)$$

$$s\hat{v} = -\theta_0^2 D_1 m^2 \hat{v} - \alpha \bar{\beta} \left(-V_1\hat{\theta} + \hat{v} + \frac{V_0}{\rho_0 + W_0}\hat{w} \right), \quad (40)$$

$$s\hat{w} = -D_2 m^2 \hat{w} + \alpha \bar{\beta} \left(-V_1\hat{\theta} + \hat{v} + \frac{V_0}{\rho_0 + W_0}\hat{w} \right), \quad (41)$$

where $\bar{\beta} = \sqrt{\theta_0}\beta$ and

$$V_1 = \frac{c(V_{s,0} - V_{s,1})}{\theta_0(\rho_0 + W_0)} - \frac{cV_{s,0}\gamma}{\theta_0(\rho_0 + W_0)}.$$

Rearrange in the matrix form, we obtain

$$M\mathbf{y} = s\mathbf{y}$$

where

$$\mathbf{y} = \begin{pmatrix} \hat{\theta} \\ \hat{v} \\ \hat{w} \end{pmatrix}, \quad M = \begin{pmatrix} -\frac{m^2}{\rho_0 + W_0} - \bar{\beta}V_1 & \bar{\beta} & \bar{\beta}\frac{V_0}{\rho_0 + W_0} \\ \alpha\bar{\beta}V_1 & -\theta_0^2 D_1 m^2 - \alpha\bar{\beta} & -\alpha\bar{\beta}\frac{V_0}{\rho_0 + W_0} \\ -\alpha\bar{\beta}V_1 & \alpha\bar{\beta} & -D_2 m^2 + \alpha\bar{\beta}\frac{V_0}{\rho_0 + W_0} \end{pmatrix}.$$

4.1 A Special Case

We want to find out whether instability would occur in this system. This requires us to consider eigenvalues of above system. To avoid complexity in calculation we consider a special case where the linearized diffusion coefficients of temperature and liquid water are same, i.e.

$$\frac{1}{\rho_0 + W_0} = \theta_0^2 D_1. \quad (42)$$

For our choice of parameters in this bread-baking problem these two coefficients are of same scale. So we expect that this assumption would not influence much the stability result of the system. Under this assumption the eigenvalue satisfies the following equation

$$\begin{aligned} (\theta_0^2 D_1 m^2 + s) \left[s^2 + \left(D_2 m^2 + \theta_0^2 D_1 m^2 + \bar{\beta} V_1 + \alpha \bar{\beta} - \frac{\alpha \bar{\beta} V_0}{\rho_0 + W_0} \right) s \right. \\ \left. + D_2 m^2 (\theta_0^2 D_1 m^2 + \bar{\beta} V_1 + \alpha \bar{\beta}) - \frac{\alpha \bar{\beta} V_0}{\rho_0 + W_0} \theta_0^2 D_1 m^2 \right] = 0. \end{aligned} \quad (43)$$

The three eigenvalues can then be calculated easily.

4.1.1 Reaction-only

When there is no diffusion, we have $m = 0$, and the eigenvalues are $s_1 = s_2 = 0$ and

$$s_3 = -\alpha \bar{\beta} - \left(\frac{V_1}{V_0} - \frac{\alpha}{\rho_0 + W_0} \right) \bar{\beta} V_0.$$

For our problem, $\alpha = 0.2864$, $\gamma = 9.662$, $\rho_0 = 0.5986$, $\theta_0 = 1.6116$ and $W_0 = 0.4$. Thus, $s_3 < 0$ and the constant solution is stable. Note that for this case the assumption that diffusion coefficients of temperature and liquid water are the same is satisfied.

4.1.2 Reaction-diffusion

We can easily see the eigenvalue associated with the first factor of above eigenvalue equation is negative. Note that the coefficient of s in the second factor

$$C_1 = D_2 m^2 + \theta_0^2 D_1 m^2 + \bar{\beta} V_1 + \alpha \bar{\beta} - \frac{\alpha \bar{\beta} V_0}{\rho_0 + W_0} > 0.$$

The signs of two eigenvalues associated with the second factor is determined by the sign of the coefficient of s^0 :

$$C_0 = D_2 m^2 (\theta_0^2 D_1 m^2 + \bar{\beta} V_1 + \alpha \bar{\beta}) - \frac{\alpha \bar{\beta} V_0}{\rho_0 + W_0} \theta_0^2 D_1 m^2$$

since the eigenvalues from the second factor is given by $-C_1 \pm \sqrt{C_1^2 - 4C_0}$. So if $C_0 < 0$ and $C_1^2 > 4C_0$, we will have a positive eigenvalue and indicates instability of the system.

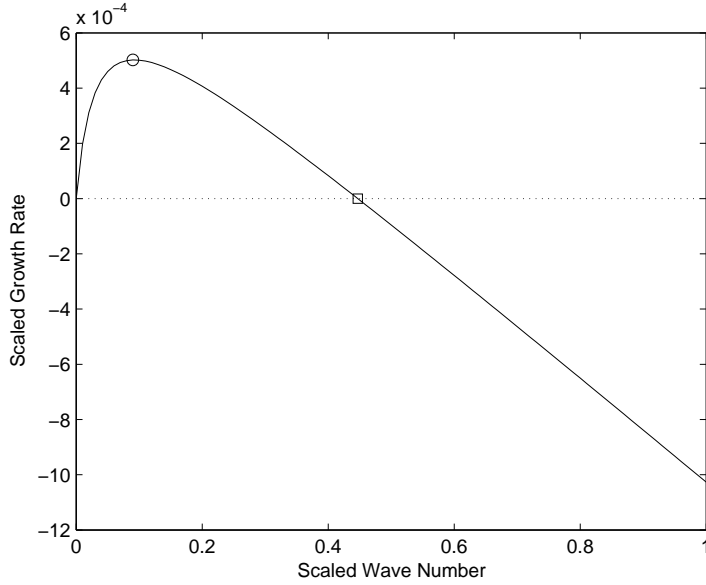


Figure 5: Plot of the normalized eigenvalue \bar{s} v.s. the normalized wave number \bar{m} . The circle indicates the most unstable wave number $\bar{m}_{max} = 0.09$. The square indicates the up-limit of the unstable modes, $\bar{m}_b = 0.4469$.

If D_2 is comparable to D_1 then C_0 will be positive and both eigenvalues will be negative and then the system is stable. But for our case D_2 is much smaller than D_1 . Hence C_0 will be negative if m is not sufficiently large, that is, we will have one positive eigenvalue which causes instability. That is why we observe instability in our computation.

Remark. It is interesting to note that in this case diffusion is actually destabilizing! From the analysis this instability depends on the diffusion coefficients D_1 and D_2 and thus may be very much related to the oscillation observed in the computation.

4.2 The General Case

In the case when diffusion coefficients for the temperature and vapor equations are not the same, analytical expression can still be obtained. However, the formula is too complicated to provide useful insights. We can nevertheless find the eigenvalues numerically by using a Matlab routine `eig.m`. Again, for the relevant parameter values two of the three eigenvalues have non-positive real parts. The real part of the third eigenvalue is plotted in Figure 5 where both the wave number and the eigenvalue are normalized as $\bar{s} = s/\bar{\beta}$ and $\bar{m} = m^2/\bar{\beta}$. It can be seen that there exists a range of wave numbers between zero and a finite value in which the perturbation will grow. Higher frequency disturbances beyond the critical wave number will not grow. Furthermore, there exists a frequency which grows the fastest, indicated by

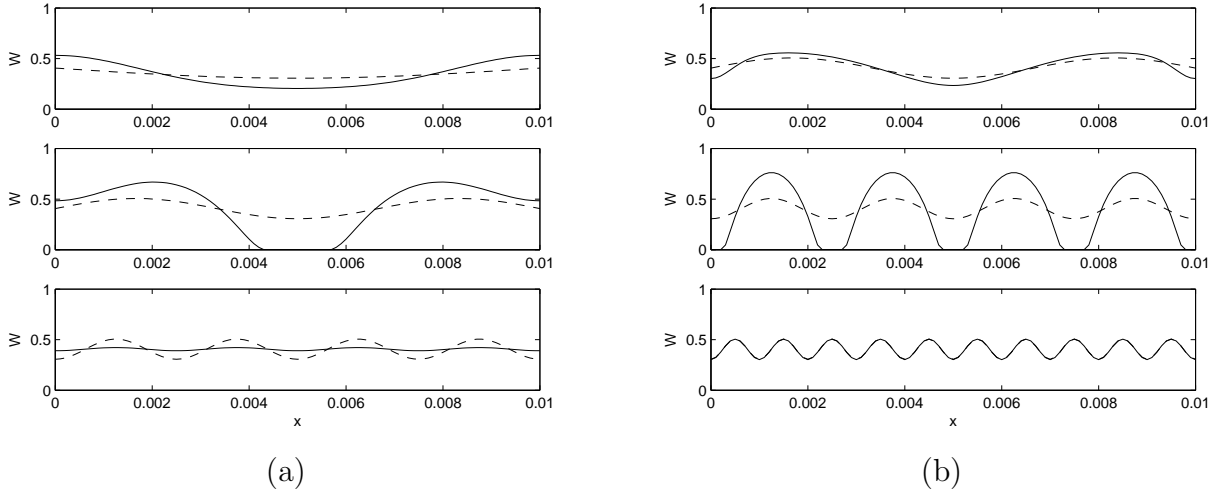


Figure 6: *Computational results of liquid water content subjected to disturbances. (a) $E = 0.0045$ with $\omega = 0.5, 1.5$ and 4 . (b) $E = 0.045$ with $\omega = 1.5, 4$ and 10 . The dashed lines indicate the initial states and the solid lines are the final solutions.*

the circle in the figure. Finally, the range of unstable frequencies increase linearly with $\sqrt{\bar{\beta}}$ and the growth rate increases linearly with $\bar{\beta}$. Therefore, a larger evaporation rate E (implies a larger $\bar{\beta}$) leads to a wider range of unstable modes and faster growth rates for all the unstable modes.

We now verify the linear stability analysis by solving the reaction-diffusion model with the Dirichlet conditions which permit the constant solution $\theta = 0$, $V = V_0$ and $W = W_0$. In Figure 6a, the computed liquid water content at the end of 100 minutes is shown. The solutions are obtained by superimpose a small disturbance in the form of $\epsilon \cos[m(\xi - 0.5)]$ to the constant liquid water content W_0 with $m = 2\pi\omega$ and $\omega = 0.5, 1.5$, and 4 . The evaporation rate is $E = 0.0045$ and the range of unstable frequencies is $0 < \omega < 2.9738$. The most unstable mode is given by $\omega \approx 1.3345$ and the rate of growth is approximately $\exp(3.5056 \times 10^{-4}t)$. The results show that even though the disturbances with wave numbers below $\omega \approx 3$ grow with time, it takes a relatively long period of time (on the scale of 80 minutes for the fastest growing mode) to develop. On the other hand, the evaporation of all the liquid water takes about 60 minutes (Figure 3). So our simulation is completed before the instability develops and takes effect.

In Figure 6b, the computed liquid water content at the end of 10 minutes is shown for a larger evaporation rate $E = 0.045$. In this case, the range of unstable frequencies is $0 < \omega < 9.4$. The most unstable mode is given by $\omega \approx 4.22$ and the rate of growth is approximately $\exp(3.5056 \times 10^{-3}t)$. The results show a much more rapid growth for the most unstable mode, on the order of 10 minutes. The difference in the growth rates for the two evaporation rates can be seen in Figure 7 where the liquid water content in the middle of the domain is plotted. The prediction using the linear stability analysis is also plotted.

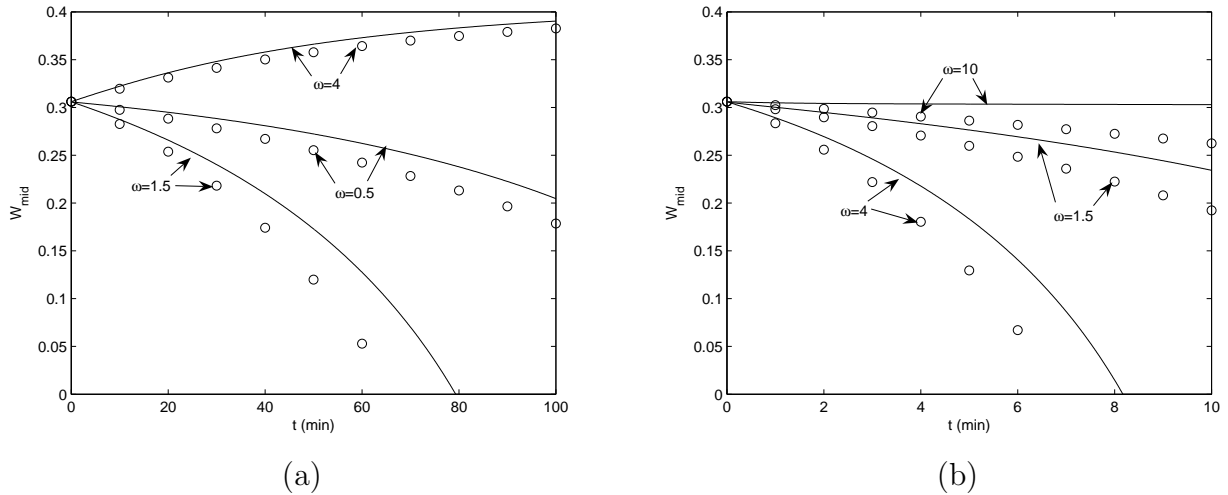


Figure 7: *Damping rates for (a) $E = 0.0045$ and (b) $E = 0.045$. The liquid water content in the middle of the domain where the growth is the fastest is plotted for wave numbers $\omega = 0.5, 1.5$ and 4 in (a) and $\omega = 1.5, 4$ and 10 in (b). The circles are predictions by the linear stability analysis.*

Note that the linear stability analysis is only valid near the constant state. Nevertheless, the two sets of data are not too far off. Thus, subject to random perturbation, the initially uniform two-phase region will become unstable. The fastest growing mode eventually causes a multiple region of dry and two-phase region, as shown in Figure 4.

Remark. From the analysis we see that the diffusive instability occurs for any positive β . However, for relatively small β computational results in the previous section are satisfactory. The reason is that the positive eigenvalue is small as β is relatively small and the disturbances develop slowly. In addition, the oscillation (diffusive instability) is only visible when the wave length of the unstable modes are shorter than the domain size in x . This explains why no oscillation occurs for the case of the smaller E .

5 Conclusion

In this paper we have re-examined the multiphase model for bread baking proposed in [18]. This model allows simultaneous heat, vapor and liquid water transfer by assuming that the phase change is instantaneous. However, previous study [15, 22] showed that this model only produces reasonable solutions for specific choices of the grid and time step sizes. Reducing the grid and time step sizes usually lead to numerical instability and cause the solution to blow up.

By constructing a reaction-diffusion model and establishing a link between the two mod-

els, we have identified the source of the instability associated to the instantaneous phase change model. We have shown that the instability observed in [15, 22] is a combination of two factors: the numerical instability as well as a diffusive instability. Using the reaction-diffusion model, we showed that the numerical instability can be eliminated by using a sufficiently small time step. This is due to the fact that the reaction-diffusion model separates the numerical instability from the diffusive instability. The diffusive instability, on the other hand, is an intrinsic feature of the model, as demonstrated by the linear stability analysis and numerical tests. For relatively large evaporation rate, the diffusive instability leads to a oscillation of solutions with multiple regions of dry and two-phase zones.

Our analysis of the reaction-diffusion model also reveals that the diffusive instability is related to the value of the evaporation rate, which is affected by the properties of the porous medium, such as the surface area of the pore space. This suggests that the phenomenon related to diffusive instability may be realized in the physical process of bread baking. Further experimental investigation is necessary to validate or invalidate the models studied in this paper.

Acknowledgement. The authors wish to acknowledge beneficial discussions with Dr. Jonathan Wylie during the preparation of the manuscript. This work is partially supported by research grants from NSERC and MITACS of Canada (HH) and Academic Research Grants R-146-000-053-112 and R-146-000-181-112 from the National University of Singapore (PL and WZ).

References

- [1] D. Alemani, B. Chopard, J. Galceran, and J. Buffle, LBGK method coupled to time splitting technique for solving reaction-diffusion processes in complex systems, *Phys. Chem. Chem Phys.* 7 (2005), no. 18, 3331-3341.
- [2] G. Carey, N. Fowkes, A. Staelens and A. Pardhanani, A class of coupled nonlinear reaction diffusion models exhibiting fingering, *J. Comp. Appl. Math.* 166 (2004), 87-99.
- [3] H.S. Carslaw and J.C. Jaeger, *Conduction of Heat in Solids*, Clarendon Press, Oxford, 1959.
- [4] J. Crank, *The Mathematics of Diffusion*, Clarendon Press, Oxford, 1975.
- [5] J. Crank, *Free and Moving Boundary Problems*, Oxford University Press, Oxford, 1987.
- [6] H.S. Davis, *Theory of Solidifications*, Cambridge University Press, Cambridge, 2001.
- [7] S. Descombes, Convergence of a splitting method of high order for reaction-diffusion systems, *Math. Comp.* 70 (2000), no. 236, 1481-1501.

- [8] U. De Vries, P. Sluimer and A.H. Bloksma, A quantitative model for heat transport in dough and crumb during baking. In "Cereal Science and Technology in Sweden," ed. by N.-G. Asp. STU Lund University, Lund, 1989, p.174-188.
- [9] A.C. Fowler, *Mathematical Models in the Applied Sciences*, Cambridge University Press, 1997.
- [10] M.L. Frankel, G. Kovacic, V. Roytburd and I. timofeyev, Finite-dimensional dynamical system modeling thermal instabilities, *Physica D* 137 (2000), 295-315.
- [11] M.L. Frankel, V. Roytburd and G. Sivashinsky, A sequence of period doublings and chaotic pulsations in a free boundary problem modeling thermal instabilities, *SIAM J. Appl. Math.* 54 (1994), No.4, 1101-1112.
- [12] F. Jones, *Evaporation of Water*, CRC Press, 1991.
- [13] K.A. Landman, C.P. Please, Modelling moisture uptake in a cereal grain, *IMA J. Math. Buss. Ind.* 10 (2000), 265-287.
- [14] M.J. McGuinness, C.P. Please, N. Fowkes, P. McGowan, L. Ryder and D. Forte, Modelling the wetting and cooking of a single cereal grain, *IMA J. Math. Buss. Ind.* 11 (2000), no.1, 49-70.
- [15] Gibin G. Powathil, A heat and mass transfer model for bread baking: an investigation using numerical schemes, M.Sc. Thesis, Department of Mathematics, National University of Singapore, 2004.
- [16] R.P. Singh and D.R. Heldman, *An Introduction to Food Engineering*, 3rd Edition, Academic Press, London 2001.
- [17] K. Thorvaldsson and C. Skjoldebrand, Water diffusion in bread during baking. *Lebensm.-Wiss. u.-Technol.*, 31 (1998), 658-663.
- [18] K. Thorvaldsson and H. Janestad, A model for simultaneous heat, water and vapor diffusion. *J. Food Eng.* 40 (1999) 167-172.
- [19] Tong, C.H. and Lund, D.B., Microwave heating of baked dough products with simultaneous heat and moisture transfer, *Journal of Food Engineering*, 19 (1993), 319-339.
- [20] B. Zanoni, C. Peri and S. Pierucci, A study of the bread-baking process I: a phenomenological model, *Journal of Food Engineering*, 19 (1993), No. 4, 389-398.
- [21] B. Zanoni, C. Peri and S. Pierucci, Study of bread baking process-II: Mathematical modelling, *Journal of Food Engineering*, 23 (1994), No. 3, 321-336.
- [22] W Zhou, Application of FDM and FEM to solving the simultaneous heat and moisture transfer inside bread during baking", *International Journal of Computational Fluid Dynamics*, 19 (2005), No. 1, 73-77.

APPENDIX. Parameters for Bread Baking

The radiative heat transfer coefficient h_r is given by the following formula

$$h_r = \frac{\sigma(T_r^2 + T^2)(T_r + T)}{\epsilon_p^{-1} + \epsilon_r^{-1} - 2 + F_{sp}^{-1}} \quad (\text{A.1})$$

where σ is the Stefan-Boltzmann constant, ϵ_p and ϵ_r are the emissivities for the product and radiative sources. The shape factor is given as

$$F_{sp} = \frac{2}{\pi ab} \left(\ln \sqrt{\frac{a_1 b_1}{1 + a^2 + b^2}} + a\sqrt{b_1} \arctan \frac{a}{\sqrt{b_1}} + b\sqrt{a_1} \arctan \frac{b}{\sqrt{a_1}} - a \arctan a - b \arctan b \right), \quad (\text{A.2})$$

where

$$a = \frac{a_{sp}}{L_{sp}}, \quad b = \frac{b_{sp}}{L_{sp}}, \quad a_1 = 1 + a^2, \quad b_1 = 1 + b^2.$$

Here L_{sp} is the distance between the radiator source and the sample surface, a_{sp} and b_{sp} are the length and the width of the sample.

Most of the parameter values are given in Table 1. The condensation/evaporation rate E is not included in the table since its value is not known.

Using the parameter values listed in Table 1, the values of the nondimensional parameters can be computed and are given in Table 2.

Table 1: *Parameter values for bread baking.*

	unit	initial value	value at T and W
λ	J/kg	2.2e6	-
k	W/m K	0.07	-
ρ	kg/m ³	284	170 + 284 W
c_p	J/kg K	3500	-
h_c	W/m ² K	0.5	-
σ	J/K ⁴ m ² s	5.67e-8	-
ϵ_p	-	0.9	-
ϵ_r	-	0.9	-
R	J/mol/K	8.31	-
M	kg/mol	1.8e-3	-
D_w	m ² /s	1.35e-10	-
D_v	m ² /s	8e-7	9e-12 T^2
h_v	1/m	120	3.2e9 T^{-3}
h_w	1/m	1e-2	1.4e-3 T +2.7e-1 W -4e-4 TW -7.7e-1 W^2
T_r	K	483	-
T_a	K	483	-
T_0	K	298.15	-
\bar{T}	K	185	-
V_a	-	5.28e-5	-
W_a	-	0	-
W_0	-	0.4	-
L	m	0.01	-
a_{sp}	m	0.12	-
b_{sp}	m	0.12	-
L_{sp}	m	0.056	-
κ	1/K	0.052227	-
$P_{s,0}$	Pascal	3.5655e3	-
$P_{s,1}$	Pascal	398	-
c	-	40	-
ϕ	-	0.5	-

Table 2: *Values of nondimensional parameters.*

D_1	4.3740
D_2	1.9×10^{-3}
h_1	$5.054(\theta + \theta_0)^{-3}$
h_2	$2.6 \times 10^{-3}\theta + 2.7 \times 10^{-3}W - 7.4 \times 10^{-4}\theta W - 7.7 \times 10^{-3}W^2$
h_3	$5.13 \times 10^{-2}(\theta + 1 + 2\theta_0)[(1 + \theta_0)^2 + (\theta + \theta_0)^2]$
h_4	7.14×10^{-2}
α	0.2864
β	$3.2085 \times 10^7 E$
γ	9.662
ρ_0	5.986×10^{-1}
θ_0	1.6116